Microsyst Technol (2007) 13:751–757
DOI 10.1007/s00542-006-0268-y

TECHNICAL PAPER

Fabrication and experimental study of Al_2O_3-TiC sliders with piezoelectric nanoactuators for flying height control

Jia-Yang Juang · Rohit P. Ambekar · David B. Bogy · C. Singh Bhatia

Received: 15 July 2006 / Accepted: 13 September 2006 / Published online: 12 October 2006

Abstract A gap flying height (FH) of less than 5 nm between the read/write element and the surface of the disk is required for ultrahigh density recording. A stable and constant FH must also be sustained in the presence of altitude and temperature changes and manufacturing tolerance. A FH adjustment or controlled slider that is capable of adjusting its gap FH has been proposed previously. In this paper we demonstrate an inexpensive and low-temperature approach for integrating piezoelectric materials in the fabrication of current small form-factor Al_2O_3-TiC sliders. A bulk PZT sheet is bonded onto the back of row-bars and the sliders are separated by a standard dicing process. It requires no deep reactive-ion etching (DRIE) or high temperature processes and is suitable for mass production. A conventional design and a new special air bearing surface (ABS) design have been fabricated and tested by an optical profiler and a FH tester. A non-flying actuation stroke of 0.6–0.8 nm/V has been observed. The FH measurements showed that the ABS plays a key role in increasing the actuation efficiency, which also agrees well with the numerical analysis.

J.-Y. Juang · R. P. Ambekar · D. B. Bogy
Computer Mechanics Laboratory,
Department of Mechanical Engineering,
Unviersity of California, Berkeley, CA 94720, USA

C. S. Bhatia
Hitachi GST, 5600 Cottle Road, San Jose,
CA 95193, USA

Present Address:
J.-Y. Juang (✉)
San Jose Research Center, Hitachi GST,
San Jose, CA 95135, USA
e-mail: jia-yang.juang@hitachigst.com

1 Introduction

As the spacing between the slider and the disk decreases in hard disk drives the linear bit spacing of the magnetic recording can decrease, resulting in a higher areal density. A gap flying height of less than 5 nm between the read/write element and the surface of the disk is required for ultrahigh density recording. A stable and constant FH must also be sustained in the presence of altitude and temperature changes, manufacturing tolerance, and track-seeking motion. Furthermore, the dynamic instability caused by FH modulations (FHMs) and nanoscale adhesion forces, such as electrostatic and intermolecular forces should be minimized. Those challenges make a conventional air bearing surface (ABS) slider an unlikely choice for an areal density of 1 Tbit/in.^{2}. One potential solution is a FH adjustment or control slider that is capable of adjusting its gap FH with sub-nanometer resolution.

Due to their quick response piezoelectric materials have been proposed as active elements for adjusting the FH. Yeack-Scranton et al. (1990) proposed an active slider for contact recording, where a piezoelectric material was inserted in a channel that ran across the full width of the slider at its top rear. They experimentally demonstrated movement of the read/write element from ~200 nm to contact, but the proposed structure of piezoelectric actuator would be difficult to implement in the smaller currently used pico- or femto-sized sliders. Another approach is to bond a layer of piezoelectric material to one side of the suspension and change the FH by bending the suspension (Good et al. 1994; Liu et al. 2002). In this case the bandwidth of actuation is limited by that of the suspension dynamics,

which is much lower than that of the air bearing. Khanna et al. (1991) and then Zhang et al. (2005) reported a method of FH adjustment by bonding a bulk piezoelectric material on the backside of a slider body. The FH was adjusted by applying voltage to the piezoelectric material and thereby changing the crown and/or camber of the slider body. The structure of such sliders is simpler and it is relatively easy to fabricate but the fact that the FH is adjusted by changing the crown and/or camber contradicts the ABS design rule of reducing sensitivity of flying attitudes to these two parameters. Another approach is to utilize piezoelectrically actuated unimorph cantilever sliders. Several papers, such as Kurita et al. (2002), Kurita and Suzuki (2004), Tagawa et al. (2003), Suzuki et al. (2003), Juang et al. (2006) and Su et al. (2005), have presented active sliders made of silicon with piezoelectric unimorph cantilevers. Based on this concept Juang and Bogy (2005, 2006) developed an observer-based nonlinear compensator for dynamic control of the FH. The slider structure was simpler and could be fabricated by silicon microfabrication technology. However, the use of silicon as the slider material and the requirement of high temperature processes make it difficult to integrate with current fabrication technology.

In this paper we propose an approach for integrating piezoelectric materials in the fabrication of current small form-factor Al_2O_3-TiC sliders. Experiments using an optical profiler, dynamic FH tester (DFHT) and acoustic emission sensor (AE) were carried out to study the actuation efficiency and flying performance of two different ABS designs.

2 Fabrication

A schematic diagram of the controlled-FH slider with a unimorph piezoelectric nanoactuator is shown in Fig. 1. The slider carries a layer of piezoelectric material, which is located between the slider body and the suspension flexure. The two slits near the trailing edge are created to form a cantilever. The read/write element is located near the end of the cantilever. When an electric voltage is applied to the middle portion of the piezoelectric material the cantilever bends down or up depending on the polarity of the induced electric field, resulting in a decrease or increase of the gap FH. There are two modes of operation. In the passive mode there is no external voltage so the active cantilever rests in the original position. The gap flying height in this case may be designed to be around 10 nm, depending on the ABS design. In the active mode the cantilever is bent into close proximity of the disk with the application of a DC voltage to the middle portion of the piezoelectric material.

Figure 2 illustrates the fabrication process of these Al_2O_3-TiC sliders with piezoelectric actuators. The process starts from dicing wafers into quads and cutting them into row-bars, followed by lapping of the row-bars to the desired slider thickness. The ABS is then defined and etched by photolithography and dry-etch processes such as ion-milling and reactive-ion etching. A thin layer of diamond-like carbon (DLC) is deposited on the entire ABS to protect the read/write element from corrosion and wear. The row-bars are then bonded with 127-μm thick commercially available lead-zirconate-titanate (PZT) sheets by silver epoxy. Thin vacuum sputtered nickel electrodes are deposited on both surfaces of the PZT sheets to produce extremely low current leakage and low magnetic permeability. A standard dicing process is used to separate the PZT and to cut the row-bars into individual sliders. Since there is no deep reactive-ion etching or high temperature processes involved, the cost introduced by these additional steps can be kept low and the previously deposited read/write element will not be damaged. The sliders are then mounted onto suspensions by the use of conductive and nonconductive glues to complete the suspension-gimbal assembly (HGA). The electrodes on the suspension flexure for read/write heads are used to apply voltages to the actuator. The prototype of a fabricated Al_2O_3-TiC slider with a layer of PZT and the completed HGA are shown in Figs. 3 and 4, respectively.

3 Experimental results and discussions

Two ABS designs are investigated in this study. The first design, depicted in Fig. 5a, is a three-pad design labeled Slider A obtained from a commercial drive. The two white rectangles near the trailing edge are slits through the entire thickness of the slider. The length and width of the slits are 550 and 65 μm, respectively. Figure 5b shows the pressure profile normalized by the ambient pressure generated under Slider A. The slider is mainly supported by the high-pressure peak created by the central trailing pad, which is typically used in commercial products. The high peak pressure helps maintain the stiffness of the air bearing. However the actuation efficiency (defined as the FH reduction to stroke ratio) is limited due to the strong counter effect of air bearing push-back.

In order to increase the actuation efficiency we designed a special ABS, named Scorpion, as shown in Fig. 6a. It has four levels of etching steps and was

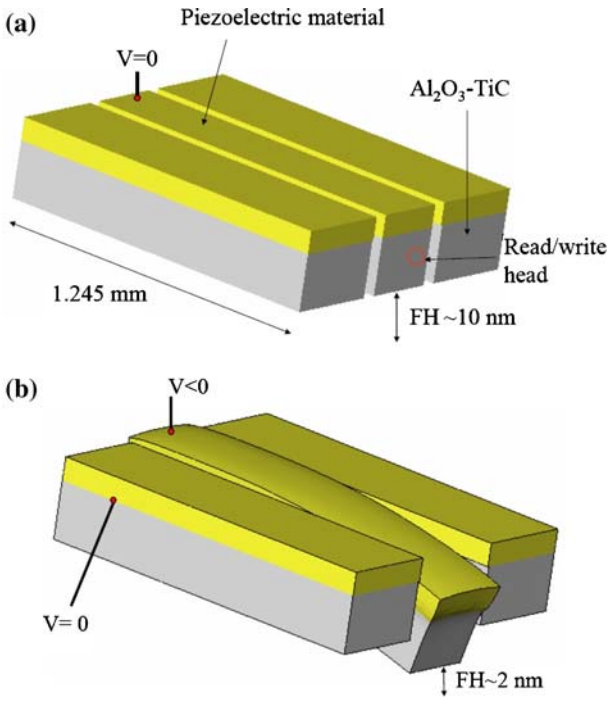

Fig. 1 Two operational modes of a FH control slider with piezoelectric actuation. **a** Passive mode, **b** active mode

designed for piezoelectric sliders with high air bearing stiffness and damping. The targeted gap FH (without actuation) is 12 nm at a disk velocity of 15,000 rpm. As shown in Fig. 6b the pressure distribution exhibits a distinct pattern compared to conventional designs. Instead of being supported by the center pressure peak the slider is primarily supported by the high pressures generated at the side pads, which significantly increases the actuation efficiency. The slits have dimensions of 65 × 600 μm. The Scorpion design was found to exhibit an overall enhancement in performance, compared with several conventional ABS designs (Juang et al. in press).

3.1 Nonflying stroke

The unimorph actuator, composed of a piece of piezoelectric material and a portion of the slider, deflects under an electric voltage V and an external vertical force F exerted on the tip. The constitutive equation of the tip deflection subject to a voltage and a force can be described as follows (Smits and Choi 1991):

$$\delta = aF + bV \tag{1}$$

$$a = \frac{1}{k_s} = \frac{4L^3}{E_p w t_p^3} \frac{\alpha\beta(1+\beta)}{\alpha^2\beta^4 + 2\alpha(2\beta + 3\beta^2 + 2\beta^3) + 1}$$

$$b = \frac{3L^2}{t_p^2} \frac{\alpha\beta(1+\beta)}{\alpha^2\beta^4 + 2\alpha(2\beta + 3\beta^2 + 2\beta^3) + 1} d_{31}$$

$$\alpha = \frac{E_s}{E_p}, \quad \beta = \frac{t_s}{t_p}$$

where the subscripts s and p stand for the slider and piezoelectric materials, respectively. E and t are the Young's modulus and beam thickness, respectively. L and w represent the length and width of the composite beam. k_s is the bending stiffness of the cantilever. d_{31} is the piezoelectric coefficient.

According to Eq. 1 the actuated stroke as a function of the cantilever length was calculated without an

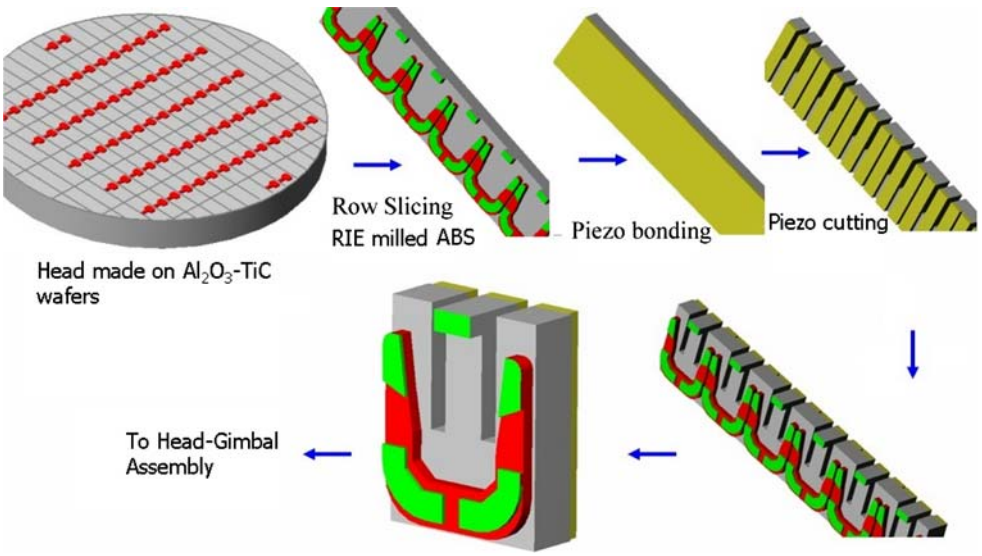

Fig. 2 Schematic diagram of the process flow

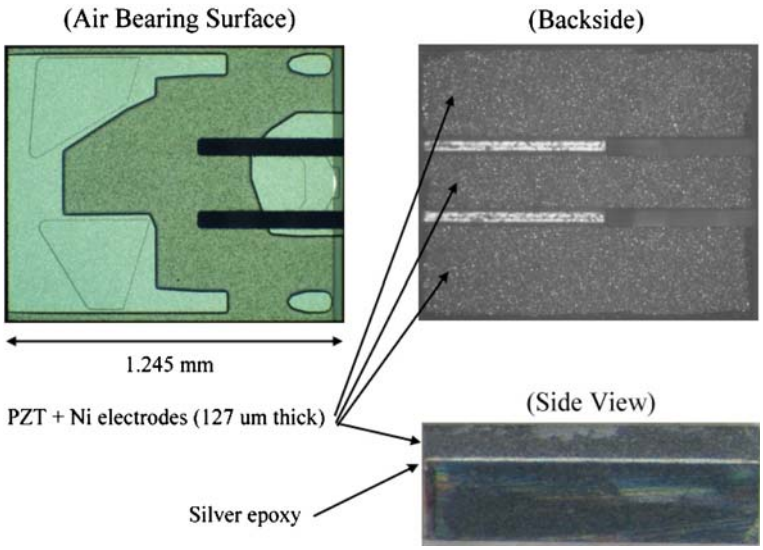

Fig. 3 An example of fabricated Al_2O_3-TiC sliders with a layer of piezoelectric material bonded on the backside

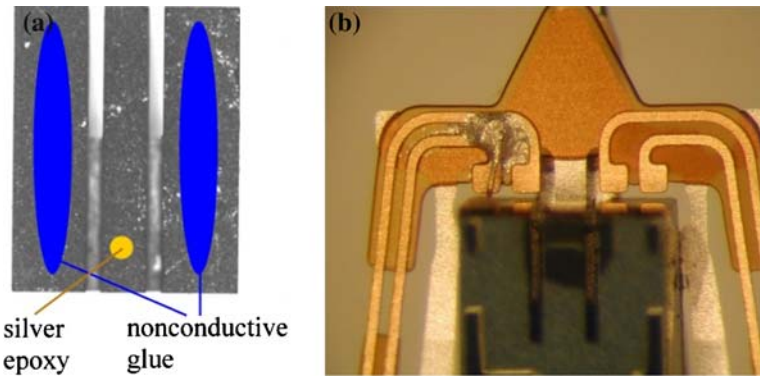

Fig. 4 HGA of the fabricated slider. **a** Conductive and nonconductive glues were used to bond the slider to the suspension. **b** The control voltage was applied to the piezoelectric material through the electrical connection

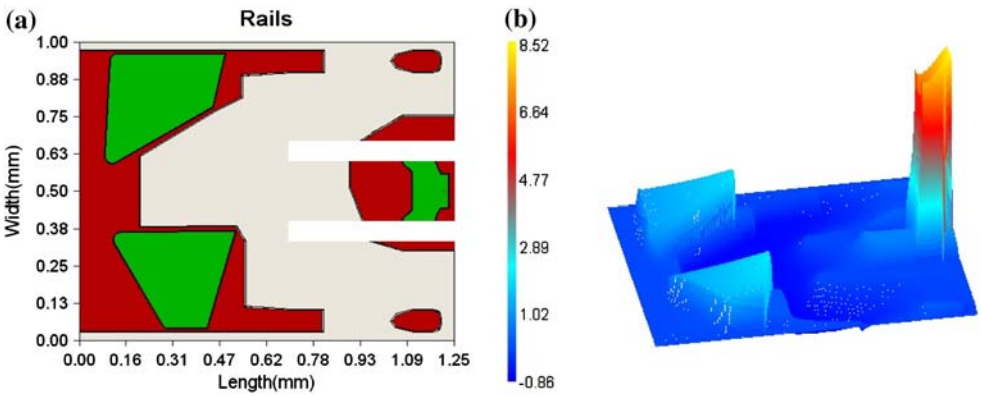

Fig. 5 **a** A pico-slider ABS used in this study. The two *white rectangles* are slits through the entire thickness of the slider. **b** Air bearing pressure profile at radial position 29.89 mm, 0° skew. The *scale* displayed is normalized to ambient pressure: $(p - p_a)/p_a$

external force. The thicknesses of the PZT and Al_2O_3-TiC layers are 127 and 300 μm, respectively. The material properties are $E_p = 62$ GPa, $E_s = 398$ GPa, $d_{31} = -320 \times 10^{-12}$ m/V. It is seen that the stroke increases as the actuator length increases and is about 0.6 nm/V for a length of 600-μm as shown in Fig. 7.

The nonflying actuated strokes of Slider A and the Scorpion slider at the pole-tip as a function of applied voltage were measured by a optical profiler. It is shown in Fig. 8 that the actuation strokes are proportional to the applied voltage with a rate of about 0.6 and 0.8 nm/V for Slider A and Scorpion, respectively. The

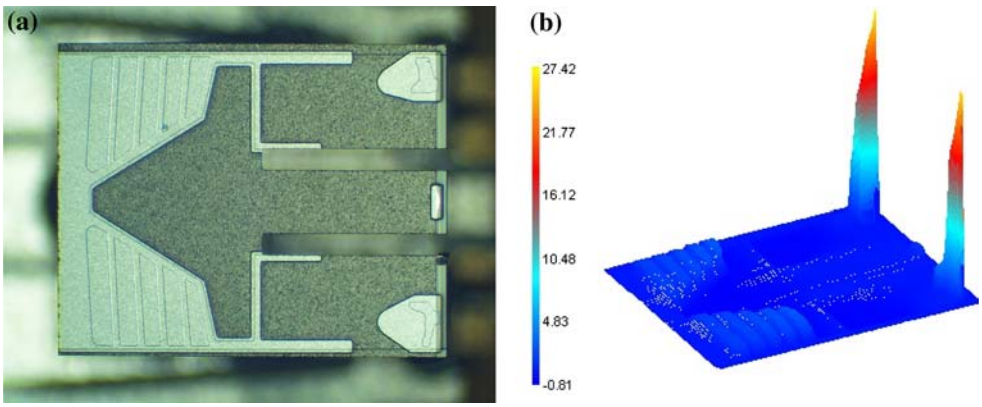

Fig. 6 **a** Fabricated Scorpion slider. The dimension of the slit is 65 × 600 μm. **b** Air bearing pressure profile at radial position 29.89 mm, 0° skew. The scale displayed is normalized to ambient pressure: $(p - p_a)/p_a$

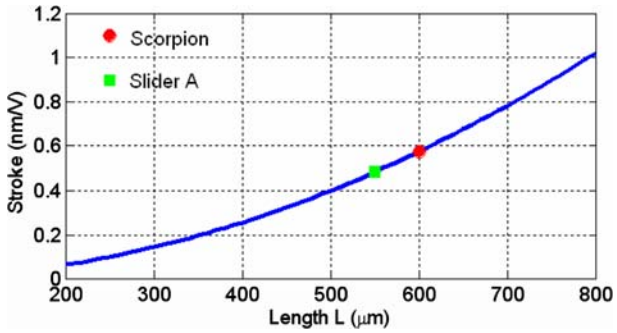

Fig. 7 Theoretical prediction of the actuated stroke of a piezoelectric unimorph actuator under 1 V. The thicknesses of the piezoelectric and Al_2O_3-TiC layers are 127 and 300 μm, respectively. The material properties are E_p = 62 GPa, E_s = 398 GPa, $d_{31} = -320 \times 10^{-12}$ m/V. The strokes are about 0.6 and 0.5 nm/V for a 600-μm and a 550-μm long cantilever, respectively

measurement data are 0.1 and 0.2 nm/V larger than the theoretical predictions for Slider A and Scorpion, respectively. This result indicates that the effective cantilever length is slightly longer than the cut length of the slits. It is also noted that an offset of –6 nm was observed for the Scorpion slider even when no voltage

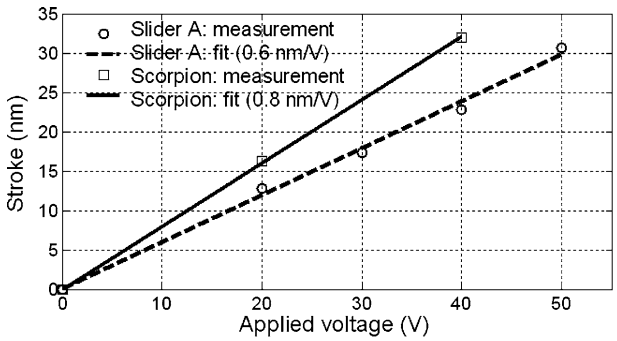

Fig. 8 Measured nonflying strokes as a function of applied voltage for Slider A and the Scorpion slider

was applied, which may be attributed to the cutting/bonding process and/or the mismatch of coefficients of thermal expansion of the PZT and Al_2O_3-TiC. It has to be taken into consideration in the FH measurements.

3.2 Flying heights: measurements and simulations

We used an optical dynamic FH tester to measure the FH of the fabricated suspended sliders. In the tests the sliders were flown over a glass disk at three radial positions (ID = 18 mm, MD = 24 mm, and OD = 30 mm) at a rotational speed of 15,000 rpm and a skew angle of 0°. For Slider A, the FHs were measured at the center trailing pad near the read/write element and the gap FHs were obtained by extrapolation. The FH change with applied voltages ranging from 0 to 50 V at the MD was measured. The experimental results are compared with numerical ones by using the CML Air Bearing Simulator with consideration of the actuation strokes obtained by the optical profiler as shown in Fig. 9. It is observed that both the experiment and simulation show a FH reduction of about 2 nm, which indicates a strong counter effect of air bearing push-back when the slider is actuated.

For the Scorpion slider the FHs were measured at the two side trailing pads. The FH at the center trailing pad could not be measured because the light spot of the instrument (~30 μm) was larger than the available area of the center pad. Instead of direct measurements the gap FHs of Scorpion were estimated by averaging the FHs at the two side-pads and taking the offset into account. The experimental and numerical results for both Slider A and Scorpion are summarized in Table 1. The measurements were conducted at the center and outer trailing pads for Slider A and the Scorpion slider, respectively. It is noted that the experimental and numerical results agree well with each other for Slider A while the measured values for Scorpion are about 2 nm smaller than those obtained by simulations. Such

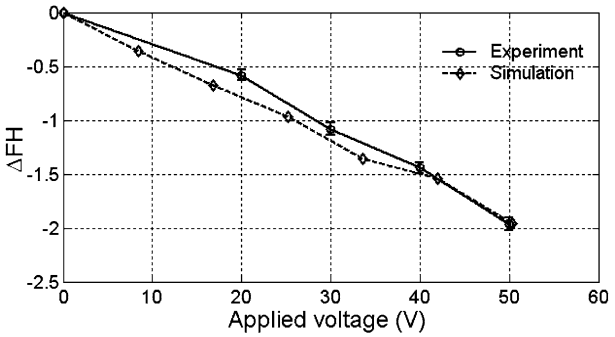

Fig. 9 Comparison of gap FH reduction of Slider A between the experimental and numerical results (15,000 rpm, 29.89 mm, 0° skew). The *error bars* represent one standard deviation from corresponding mean values

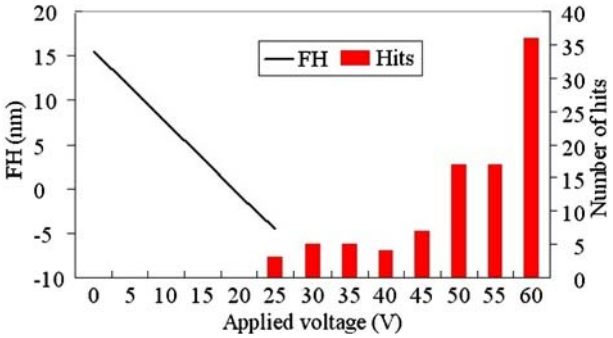

Fig. 10 The number of hits (spikes) and the estimated FH of the Scorpion slider as functions of the applied voltage. The contact event that has an AE amplitude over ±500 mV was counted as a hit

a discrepancy may be attributed to measurement inaccuracy due to calibration (Watanabe and Aruga 2006). Based on the results, the gap FHs of Slider A and Scorpion at the MD are estimated to be 44.53 and 15.5 nm, respectively.

3.3 Contact tests

Contact tests were conducted on an Optical Surface Analyzer (OSA) spin-stand with an AE sensor for detecting contact. A smooth disk (rms = 0.2 nm) with 12Å Zdol 4000 lubricant was used in these tests. The Scorpion slider was loaded on the disk at a radial position of 26 mm and a linear speed of 38 m/s. The slider body was grounded and an electrical voltage was applied to the top electrode of the piezoelectric actuator. The voltage was gradually increased from 0 to 60 V at an increment of 5 V. Isolated spikes of AE signals were observed when a voltage of over 25 V was applied to the actuator. These spikes were caused by the intermittent contacts of the center pad and the disk. However, such a pattern of the AE signals during contact is different from that observed in the conventional sliders during ''touchdown-takeoff tests'' (Ambekar and Bogy 2005) where there was a pronounced increase in the amplitude of the AE signal upon contact. Therefore during controlled contact (as is the case here) only a small portion of the slider comes into contact with the disk while the rest of the ABS is supported by the air bearing. There is no loss of air bearing as the voltage increases to increase the intensity of contact. Hence the corresponding AE signal showed only an increase in the frequency of contacts but not an AE avalanche which occurs in case of conventional sliders when complete loss of the air bearing occurs.

Figure 10 shows the number of hits (spikes) and estimated FH as functions of the applied voltage. Any contact event that has an AE amplitude over ±500 mV was counted as a hit. No such contact event was detected by the AE sensor when the applied voltage was less than 20 V, corresponding to a FH of –0.5 nm and contact events were first detected when the applied voltage was increased to 25 V, corresponding to a FH of about –4.5 nm. A monotonic increase in the number of hits was observed as the voltage was increased, which indicates that the event of intermittent contacts became more frequent when the actuated stroke of the center pad was increased. It is noted that the contact was first detected at a FH between –0.5 and –4.5 nm, which was less than the take-off height (~2 nm). There are three possible reasons: one may be attributed to the AE sensor which may not be sensitive enough to detect the slight contact. Another may be due to the measurement method using the conventional unload calibration which tends to underestimate the FH by 2 nm. The third may be the

Table 1 Comparisons of the simulated and measured FHs of Slider A and Scorpion

	Outer diameter		Middle diameter		Inner diameter	
	Simulated (nm)	Experimental (nm)	Simulated (nm)	Experimental (nm)	Simulated (nm)	Experimental (nm)
Slider A (center trailing pad)	43.10	44.53 (1.65)	40.78	40.69 (1.10)	38.26	36.81 (1.43)
Scorpion (outer trailing pad)	13.31	11.64 (0.2)	13.43	10.04 (0.18)	13.11	11.01 (0.18)

The values in the parentheses are the standard deviations

push-back lifting force generated by the center trailing pad, which may reduce the actuation stroke as compared to the case without flying.

4 Conclusions and future work

This paper proposes a low-temperature and inexpensive process for fabricating and integrating Al_2O_3-TiC sliders with piezoelectric nanoactuators. The measured nonflying actuation stroke exhibits a linear relationship with the applied voltage with a rate of 0.6–0.8 nm/V. In addition, the flying height measurements showed that the ABS design played a key role in increasing actuation efficiency, which also agreed well with the numerical analysis. The actuation efficiency of a conventional design, Slider A, is found to be only 7%, which indicates a strong air bearing coupling with the actuation. The FH of the Scorpion slider was successfully reduced from about 15.5 nm to contact with an applied voltage of 20 V, which demonstrated high actuation efficiency.

Another advantage of the proposed technology is in the ability to sense contact/airbearing behavior through the combination of inverse and direct piezo effects. Sectioned/deposited electrodes on the piezo element could produce a sensor performing in-situ acoustic emission (AE) type sensing (Ragulskis 1988; Uchino 1997). Some potential manufacturing/operation issues include: 1. Manufacturability of the piezo slider. Manufacturability of the piezo element in the slider production line, ensuring repeatable slider cutting operation, which is critical for the piezo actuator performance. 2. PZT material in the drive. Despite the fact that there were several implementations of piezo material inside the drive, compatibility of the lead-zirconium-titanate with the modern lubricant systems has to be investigated. 3. PZT particles generated right at the head-disk-interface by the piezo actuator while adjusting FH. All these potential manufacturing issues have to be studied in the future.

Acknowledgments This study is supported by the Computer Mechanics Laboratory (CML) at University of California, Berkeley and the Information Storage Industry Consortium (INSIC). J. Y. Juang has also been supported by The California State Nanotechnology Fellowship. The authors would like to thank T. Neumann, Y. Midori, N. Bach and V. Chow of Hitachi Global Storage Technology for assistance in the fabrication, measurements and useful discussions. This work was originally presented in the 2006 ASME/JSME Joint Conference on Micromechatronics for Information and Precision Equipment, June 21–23, 2006, Santa Clara, CA, USA.

References

Ambekar RP, Bogy DB (2005) Effect of slider lubricant pickup on stability at the head-disk interface. IEEE Trans Magn 41:3028–3030

Good DL, Mason JE, Ottesen HH (1994) Fly height servo control of read/write head suspension. U.S. Patent 5 377 058, December 27

Juang JY, Bogy DB (2005) Controlled-flying proximity sliders for head-media spacing variation suppression in ultralow flying air bearings. IEEE Trans Magn 41:3052–3054

Juang JY, Bogy DB (2006) Nonlinear compensator design for active sliders to suppress head-disk spacing modulation in hard disk drives. IEEE ASME Trans Mechatron 11:256–264

Juang JY, Bogy DB, Bhatia CS Design and dynamics of flying height control slider with piezoelectric nanoactuator in hard disk drives. J. Tribol (in press)

Juang JY, Chen D, Bogy DB (2006) Alternate air bearing slider designs for areal density of 1 Tb/in^2. IEEE Trans Magn 42:241–246

Khanna VD, Hendriks F, Praino AP (1991) Programmable air bearing sliders. IEEE Trans Magn 27:5145–5147

Kurita M, Suzuki K (2004) Flying-height adjustment technologies of magnetic head sliders. IEEE Trans Magn 40:332–336

Kurita M, Yamazaki T, Kohira H, Matsumoto M, Tsuchivama R, Xu J, Harada T, Inoue Y, Su L, Kato K (2002) An active-head slider with a piezoelectric actuator for controlling flying height. IEEE Trans Magn 38:2102–2104

Liu X, Li A, Clegg W, Jenkins DFL, Davey P (2002) Head–disk spacing variation suppression via active flying height control. IEEE Trans Instrum Meas 51:897–901

Ragulskis K (1988) Vibromotors for precision microrobots. New York: Hemisphere

Smits JG, Choi WS (1991) The constituent equations of piezoelectric heterogeneous bimorphs. IEEE Trans Ultrason Ferroelectr Freq Control 38:256–270

Su L, Kurita M, Xu J, Kato K, Adachi K, Miyake Y (2005) Static and dynamic characteristics of active-head sliders. Tribol Intl 38:717–723

Suzuki K, Maeda R, Chu J, Kato T, Kurita M (2003) An active head slider using a piezoelectric cantilever for in situ flying-height control. IEEE Trans Magn 39:826–831

Tagawa N, Kitamura KI, Mori A (2003) Design and fabrication of MEMS-based active slider using double-layered composite PZT thin film in hard disk drives. IEEE Trans Magn 39:926–931

Uchino K (1997) Piezoelectric actuators and ultrasonic motors. Dordrecht, Netherlands, Kluwer Academic Publishers

Watanabe T, Aruga K (2006) A study of flying height measurement accuracy for under 10-nm spacing. In: Proceedings of ASME/JSME Joint Conference on Micromechatronics for Information and Precision Equipment, 21–23 June 2006, Santa Clara, CA, USA

Yeack-Scranton CE, Khanna VD, Etzold DF, Praino AP (1990) An active slider for practical contact recording. IEEE Trans Magn 26:2478–2483

Zhang M, Yu S, Liu J, Liu B (2005) Flying height adjustment by slider's air bearing surface profile control. J Appl Phys 97:10 P309